Title

Large remodeling of the Myc-induced cell surface proteome in B cells and prostate cells creates new opportunities for immunotherapy

Journal

Proceedings of the National Academy of Sciences of the United States of America, 118(4)

ISSN

0027-8424

Authors

Chen, Wentao
Mou, Kurt Yun
Solomon, Paige
et al.

Publication Date

2021-01-26

DOI

10.1073/pnas.2018861118

Peer reviewed

Large remodeling of the Myc-induced cell surface proteome in B cells and prostate cells creates new opportunities for immunotherapy

Wentao Chen[a,b,1], Kurt Yun Mou[a,c,1], Paige Solomon[a], Rahul Aggarwal[d], Kevin K. Leung[a], and James A. Wells[a,e,2]

[a]Department of Pharmaceutical Chemistry, University of California, San Francisco, CA 94158; [b]Department of Therapeutic Discovery, Amgen Research, Thousand Oaks, CA 91320; [c]Institute of Biomedical Sciences, Academia Sinica, Taipei, Taiwan 11529; [d]Department of Medicine, University of California, San Francisco, CA 94158; and [e]Department of Cellular and Molecular Pharmacology, University of California, San Francisco, CA 94158

Edited by Owen N. Witte, David Geffen School of Medicine at University of California, Los Angeles, CA, and approved December 2, 2020 (received for review September 8, 2020)

MYC is a powerful transcription factor overexpressed in many human cancers including B cell and prostate cancers. Antibody therapeutics are exciting opportunities to attack cancers but require knowledge of surface proteins that change due to oncogene expression. To identify how MYC overexpression remodels the cell surface proteome in a cell autologous fashion and in different cell types, we investigated the impact of MYC overexpression on 800 surface proteins in three isogenic model cell lines either of B cell or prostate cell origin engineered to have high or low MYC levels. We found that MYC overexpression resulted in dramatic remodeling (both up- and down-regulation) of the cell surfaceome in a cell type-dependent fashion. We found systematic and large increases in distinct sets of >80 transporters including nucleoside transporters and nutrient transporters making cells more sensitive to toxic nucleoside analogs like cytarabine, commonly used for treating hematological cancers. Paradoxically, MYC overexpression also increased expression of surface proteins driving cell turnover such as TNFRSF10B, also known as death receptor 5, and immune cell attacking signals such as the natural killer cell activating ligand NCR3LG1, also known as B7-H6. We generated recombinant antibodies to these two targets and verified their up-regulation in MYC overexpression cell lines and showed they were sensitive to bispecific T cell engagers (BiTEs). Our studies demonstrate how MYC overexpression leads to dramatic bidirectional remodeling of the surfaceome in a cell type-dependent but functionally convergent fashion and identify surface targets or combinations thereof as possible candidates for cytotoxic metabolite or immunotherapy.

oncogenes | glycoproteomics | surfaceome | MYC | antibody

MYC is a powerful transcription factor controlling the expression of >1,000 different genes, many of which are involved in biosynthesis processes (1, 2). Overexpressed MYC is a driving oncogene that contributes to the genesis and progression of many human cancers (3–7). In normal tissues, the expression of the MYC protein is tightly regulated by a number of mechanisms that control promoter activity, RNA polymerase elongation, and mRNA processing (8). However, its deregulation occurs frequently in human cancers as the MYC promoter is targeted by various cancer-associated signal transduction cascades, including WNT, RAS/RAF/MAPK, and NF-κB pathways (8, 9).

MYC's role in human cancer was first discovered in Burkitt's lymphoma where MYC expression is altered by chromosomal translocation (10–12). MYC amplification and MYC protein overexpression have also been found in prostate cancer (PC), ovarian cancers, and hepatocellular carcinoma and in a high percentage of lung cancers (13). In PC, MYC amplification and MYC overexpression happen in both primary and metastatic disease. Focal amplification of the region spanning MYC creates a genetic defect commonly observed in 8% of primary PC that results in MYC overexpression (14–17). This event happens four to five times more frequently in lethal metastatic castrate-resistant prostate cancer (mCRPC) (14, 18–20). MYC overexpression can also be triggered by other genetic and epigenetic defects such as TMPRSS2-ERG fusion (21), a tandem duplication of the regulatory loci upstream of MYC (18). Mechanistically, MYC promotes oncogenic signaling in PC and stimulates cell growth by up-regulating the expression of a number of factors involved in cell growth and proliferation (22). Several studies in transgenic mouse models demonstrate that inactivating MYC can cause tumor regression, suggesting that inhibition of MYC expression or activity may be useful in treating cancer patients (4, 23, 24). However, drug development aimed at targeting MYC directly has proved challenging given that MYC is intrinsically disordered and forms heterodimeric helical structures with few surface features compatible for binding small molecules (25). There are also concerns over targeting the MYC protein directly as it is an important factor for normal tissue renewal and homeostasis (26). Other small molecule approaches

Significance

MYC is a powerful transcription factor and when overexpressed can drive cancers. We broadly characterized the MYC-driven surfaceome in B cells and prostate cells using proteomics. MYC overexpression induces large bidirectional changes in the surfaceome through broad up-regulation of >80 metabolite transporters important for cell proliferation and paradoxical up-regulation of two receptors involved in cell turnover such as a TNF receptor family member and a natural killer cell activating ligand. We targeted these two receptors using recombinant bispecific T cell engagers (BiTEs) to kill MYC overexpressing cells. These cells are also more sensitive to toxic nucleosides to two up-regulated nucleoside transporters. Our studies identify surface targets or combinations thereof as possible candidates for immunotherapy or cytotoxic metabolites.

Author contributions: W.C., K.Y.M., K.K.L., and J.A.W. designed research; W.C., K.Y.M., P.S., and K.K.L. performed research; R.A. contributed new reagents/analytic tools; W.C., K.Y.M., P.S., and K.K.L. analyzed data; and W.C., K.Y.M., R.A., K.K.L., and J.A.W. wrote the paper.

Competing interest statement: K.K.L. and J.A.W. received research funding from Celgene Corporation but no personal financial gain or equity.

This article is a PNAS Direct Submission.

[1]W.C. and K.Y.M. contributed equally to this work.

[2]To whom correspondence may be addressed. Email: jim.wells@ucsf.edu.

This article contains supporting information online at https://www.pnas.org/lookup/suppl/doi:10.1073/pnas.2018861118/-/DCSupplemental.

Published January 22, 2021.

have indirectly targeted consequences of MYC by interfering with the MYC transcriptional program [BET bromodomain inhibitors (27, 28)] or targeting downstream cellular events (3, 29, 30). Another approach is targeting cell surface proteins up-regulated by MYC in cancer cells. Antibody-based therapeutics could be a fruitful approach, as antibodies are highly selective and now represent 8 of the top 10 selling drugs. There are currently only about 24 surface targets for which there are approved antibody therapeutics, despite there being more that 4,000 human genes that encode membrane proteins (31, 32). Thus, discovering cell surface antigens as targets for therapies to treat MYC-driven cancers is of high interest.

Here, we broadly characterize the MYC-driven surfaceome in both B cells and prostate cells using a mass spectrometry-based proteomic approach, called cell surface capture (CSC) (33). We find MYC overexpression induces large bidirectional changes for 20 to 30% of the 500 to 800 different membrane proteins quantified. Despite differences in expression patterns among the cell types, gene set enrichment analysis reveals commonly up-regulated functions, especially those involving transporter activities that are important for cell proliferation, and paradoxically cell turnover such as TNF receptor family members and natural killer cell activating ligands. We validated the functional relevance of two up-regulated nucleoside transporters for sensitizing cells to toxic nucleosides. Furthermore, we generated high-affinity recombinant antibodies to some of the up-regulated targets and showed these can selectively induce T cell activation with high-MYC B cell lymphoma cells and prostate cells using bispecific T cell engagers (BiTEs). Our studies reveal how simple overexpression of MYC can substantially remodel the surfaceome in a cell type and cell autologous fashion and provide a resource for potential drug targets.

Results

Elevated MYC Expression Level Results in Dramatic and Bidirectional Surfaceome Remodeling in Three Isogenic Cell Lines from B Cells and Prostate Cells. To broadly profile the impact of MYC overexpression on the surfaceome, we adopted a mass spectrometry-based proteomic approach to quantitatively analyze the cell surface glycoprotein expression. We began by analyzing the surfaceome of P493-6 cells (34), an engineered B cell model of Burkitt's lymphoma in which MYC is overexpressed (high MYC) but can be suppressed by a tetracycline-inducible promoter by >20-fold (low MYC) (Fig. 1*A*). To quantify the changes in surface protein expression we employed stable isotope labeling by amino acids in cell culture (SILAC) (35) in which P493-6 cells were grown in media containing a mixture of heavy or light lysine/arginine with and without tetracycline to generate low-MYC and high-MYC states for 1, 2, or 3 d to follow the time course.

We were able to quantitatively compare the levels of about 500 membrane glycoproteins in both the low- and high-MYC samples taken at 1, 2, and 3 d. There was a strong correlation ($r > 0.85$) between the distribution of proteins and expression levels found over the 3-d time course (*SI Appendix*, Fig. S1); this suggests that the impact of MYC expression on the surfaceome had reached a near-steady state even after 1 d of induction and reflects the consistency of the mass spectrometry (MS) data. Rather than averaging all of the datasets, which did not differ substantially, we chose to focus on the day 3 dataset containing 494 membrane proteins detected in both the low- and high-MYC samples. A standard volcano plot (Fig. 1*B* and Dataset S1) shows large changes in expression of 2- to 10-fold up or down for 206 proteins representing about two-fifths of the detected surfaceome. These changes are bidirectional where 131 membrane proteins were up-regulated and 75 down-regulated.

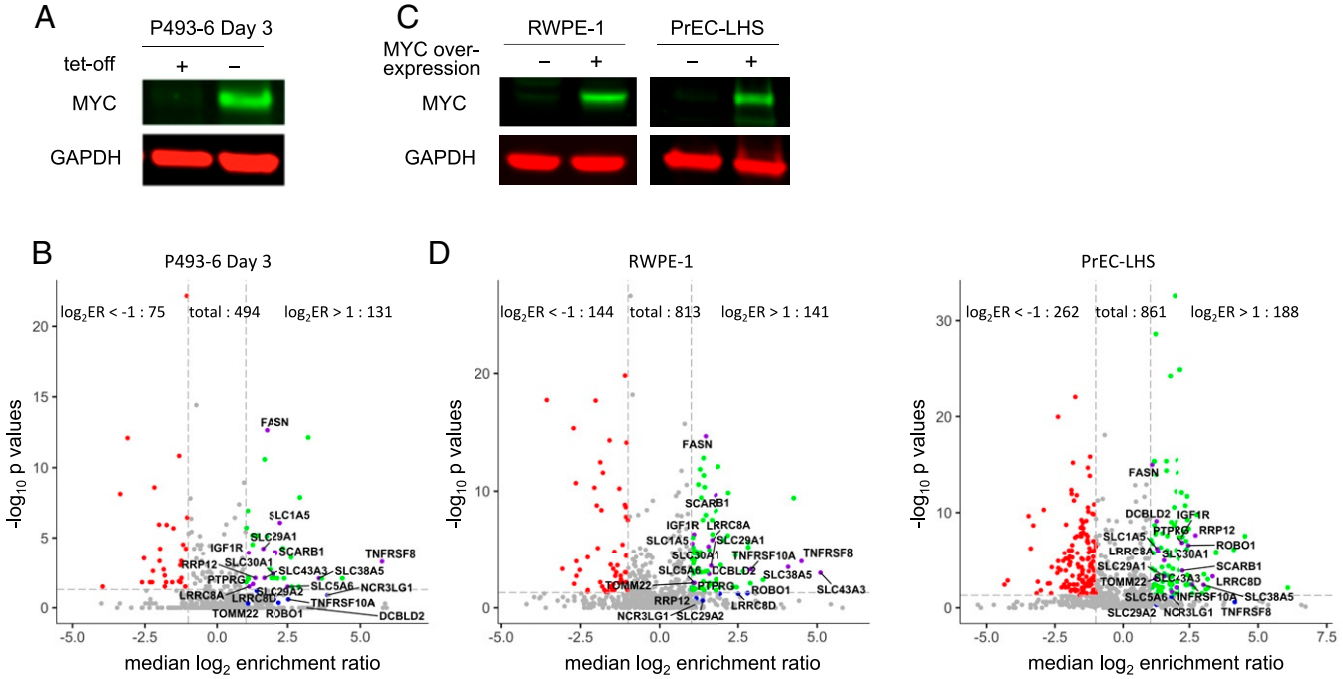

Fig. 1. Stable overexpression of MYC in an engineered B cell line (P493-6) and two prostate cell lines (RWPE-1 and PrEC-LHS) leads to large and bidirectional changes in the cell surfaceome. (*A*) Induction of MYC in P493-6 cells upon removal of tetracycline leads to >20-fold induction of MYC by Western blotting. A total of 20 μg cell lysate was loaded to each lane. GAPDH was used as the loading control. (*B*) Volcano plot showing bidirectional remodeling of cell surface proteome of high versus low MYC in P493-6 cells. Surface proteins with $\log_2$ enrichment ratio (ER) < 1, *P* value < 0.05 and $\log_2$ ER > 1, *P* value < 0.05 are shown as red and green dots, respectively. The 20 commonly up-regulated proteins are labeled and shown as purple ($P < 0.05$) and blue ($P > 0.05$) dots in each plot. (*C*) Stable overexpression of MYC in RWPE-1 and PrEC-LHS cells leads to greater than fourfold increase in MYC expression by Western blot as processed above. (*D*) Volcano plots processed as in *B* showing bidirectional remodeling of surface proteins for high versus low MYC for RWPE-1 cells (*Left*) and PrEC-LHS cells (*Right*).

We next analyzed how MYC overexpression remodels the surfaceome of immortalized prostate epithelial cell lines, PrEC-LHS (36) and RWPE-1 (37). Isogenic stable cell lines with or without MYC overexpression were generated by lentiviral transduction. PrEC-LHS is a human prostate epithelial cell line infected with amphotropic retroviruses encoding the SV40 large T antigen (L), the telomerase catalytic subunit hTERT (H), and the SV40 small T antigen (S). RWPE-1 is a human prostate epithelial cell line immortalized with papillomavirus 18. Both of the cell lines are able to provide a relatively simple genetic background for our isogenic studies. MYC overexpression in these two cell lines led to more than fourfold increase in MYC levels as assessed by Western blotting (Fig. 1*C*). The cell morphologies also varied significantly from their isogenic control cell lines, reflecting the impact of MYC overexpression (*SI Appendix*, Fig. S2); the PrEC-LHS-Myc cells were less adherent, suggesting substantial changes in the surfaceomes. Due to the expense of obtaining SILAC medium for RWPE-1 cells we chemically introduced the isotopic labels by reductive dimethylation (ReDiMe) postculturing (38). Samples were processed as above except that the entire tryptic fraction from the on-bead digestion was analyzed. For the PrEC-LHS and RWPE-1 cells we identified 861 and 813 surface proteins, respectively (Fig. 1*D* and Dataset S1). MYC overexpression in these epithelial cells led to similar bidirectional remodeling showing greater than twofold changes in expression of more than 35% of the observed surfaceomes reflecting a similarly impactful state change, as was seen for the P493-6 B cells.

We next compared the three cell lines in terms of the total proteins and changes we observed to their surfaceomes (Fig. 2). In total, 862, 814, and 495 proteins were identified in PrEC-LHS, RWPE-1, and P493-6 cell surfaceomes, respectively, and a total of 1,240 proteins were identified between all three cell lines (Fig. 2*A* and Dataset S1). About 20% (250/1,240) of the identified surface proteins were in common between the three cell lines, and 14 to 16% (176 to 206 of 1,240 total proteins) were unique to each cell line. Not surprisingly, there is much greater overlap between the two prostate cell lines overexpressing MYC (613 proteins) compared to either of those with the B cells overexpressing MYC (275 and 293 proteins for RWPE-1 and PrEC-LHS, respectively). To compare significantly enriched proteins between the cell lines, an upset plot was generated to visualize the number of surface proteins up-regulated or down-regulated by more than twofold in these three cell lines (Fig. 2*B*; *SI Appendix*, Fig. S3; and Dataset S1). Although there are 20 common up-regulated proteins among the three cell lines, each cell line exhibits very distinct features. Specifically, 40% (345/862), 23.8% (194/814), and 29.9% (148/495) of the quantified surfaceome were uniquely up-regulated and down-regulated in PrEC-LHS, RWPE-1, and P493-6, respectively. The overall comparisons between the three cell lines can be quantified in the pairwise correlation plots of the SILAC ratios, with Spearman correlation *r* value ranging between 0.31 and 0.38 (Fig. 2*C* and Dataset S1). These similarities and differences can also be viewed in the heat maps for the total proteins (Fig. 2*D* and Dataset S1) and those for the set of top proteins that change most dramatically in any cell line (Fig. 2*E* and Dataset S1).

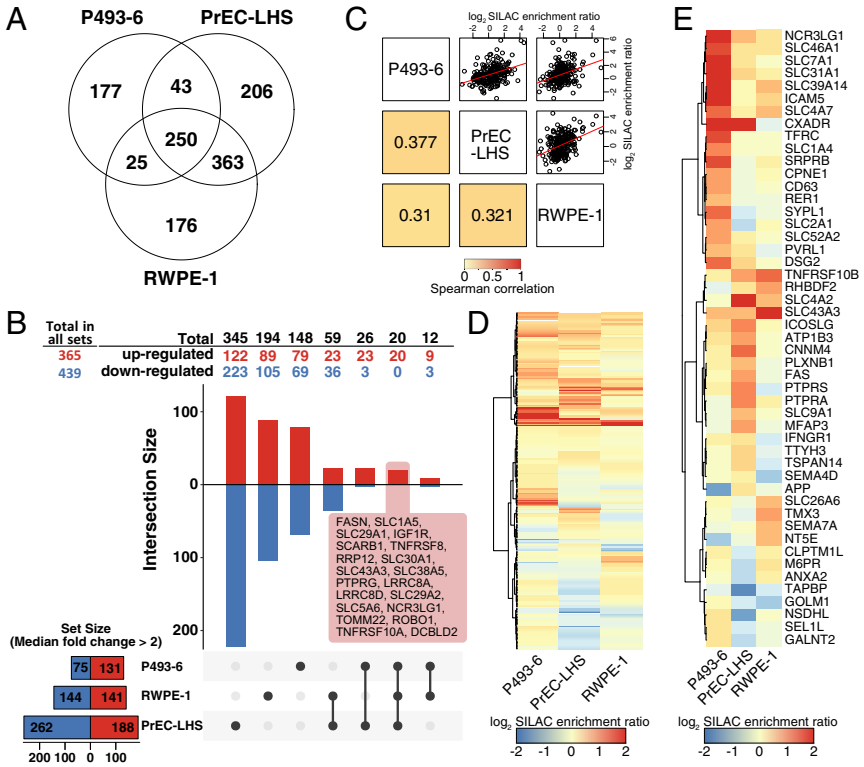

Fig. 2. Comparing the global and specific MYC-induced changes in the surfaceome for the engineered B cell line (P493-6) and the two prostate cell lines (RWPE-1 and PrEC-LHS). (*A*) Venn diagram of the observed surface proteins in the three high versus low surfaceomics MS experiments shows significant differences as well as similarities. (*B*) UpSet plot of the up-regulated (red) or down-regulated (blue) surface proteins in the three high versus low MYC surfaceomic experiments shows bidirectional remodeling and 20 commonly up-regulated proteins. (*C*) Pairwise comparison of the $\log_2$ ER for the surface proteins in the three cell lines detected in the high versus low MYC surfaceomic experiments. The correlation coefficients (Spearman) for each of the comparisons are shown in the corresponding squares and suggest a modest correlation between all three. (*D*) Hierarchal clustering of surfaceome changes revealed similarities and differences among three cell lines expressing high versus low levels of MYC. (*E*) Heatmap of the ER changes for the top most changed proteins in the three high versus low MYC surfaceomic experiments.

Thus, although MYC-induced changes do show some overlap at the individual target level, there are significant cell line-dependent differences suggesting that context is an important factor in determining the exact nature of the MYC-driven surfaceome.

Common Functional Impact of MYC Overexpression on the Surfaceome. Despite differences between the surfaceomes of the three MYC overexpressing cell lines, GeneSet enrichment analysis (GSEA) shows the changes harmonize remarkably well for the functions of the up-regulated proteins among the three cell lines, suggesting functional redundancy (Fig. 3*A* and Dataset S2). The dominant category by far is the broad up-regulation of solute and nutrient carrier proteins across all three cell lines. Small molecule metabolite and ion transporters represent over half of the functional categories that are up-regulated. For example, about 40 surface proteins in the organic acid transmembrane category were detected in our data, and more than half were significantly up-regulated in one or more cell lines (Fig. 3*B*). Similar results were seen for the sodium ion transmembrane transporter set (Fig. 3*C*) and the amino acid transporter set (Fig. 3*D*).

GeneSet analysis also identified a global enrichment of transmembrane transporter (Gene Ontology [GO]: 0055085), which further enforces that transporters are highly up-regulated in MYC-overexpressing cell lines. Of the 199 proteins identified with such annotation, 82 of these proteins were found to be up-regulated in at least one of the cell lines (*SI Appendix*, Fig. S4*A*). These conclusions were reinforced by GeneSet analysis using REACTOME showing the changes were dominated by the small molecule transporter class of proteins, summarized in *SI Appendix*, Fig. S4*B*. Moreover, 9 of the 20 commonly up-regulated proteins among the three cell lines were small molecule or ion solute carrier proteins including LRRC8A, LRRC8D, SLC1A5, SLC29A1, SLC30A1, SLC43A3, SLC38A5, SLC29A2, and SLC5A6. Two of these commonly expressed transporters, SLC29A1 and SLC29A2, are well-known transporters of nucleosides also known as equilibrative nucleoside tansporter-1 and -2, ENT1 and ENT2, that are elevated systematically from two- to fourfold in the MYC high versus low states in all three cell lines (*SI Appendix*, Fig. S4*C*. Resistance to the cytotoxic nucleoside cytarabine (Ara-C), often used in treatment of acute myeloid leukemia, can be caused by down-regulation of ENT1 (39). Thus, we tested the sensitivity to cytarabine treatment for the high- and low-MYC expressing cells (Fig. 4). Indeed, two of the cell lines overexpressing MYC, the B cell line P493-6 (Fig. 4*A*) and the prostate cell line PrEC-LHS (Fig. 4*B*), showed >10-fold higher sensitivity to cytarabine in the high-MYC state (half-maximal inhibitory concentration (IC_{50}) 3 μM in high MYC vs. >30 μM in low MYC). This higher sensitivity to Ara-C rendered by MYC overexpression was substantially blunted by adding an ENT-specific inhibitor S-(4-Nitrobenzyl)-6-thioinosine. We also tested RWPE cells and found them to be 10-fold more sensitive to cytarabine (IC_{50} 300 nM) compared to the P493-6 or PrEC-LHS cells either in low- or in high-MYC states, and the S-(4-Nitrobenzyl)-6-thioinosine inhibitor did not alleviate the cytotoxicity (Fig. 4*C*). These data suggest another transporter other than ENT1/2 may be at play for cytarabine uptake or that the RWPE cells lack efflux pumps of cytarabine that may be present in the other two cell lines.

The next category of proteins that had significantly up-regulated expression patterns were ones broadly associated with apoptosis and in particular eight receptors from the TNF receptor family (Fig. 5*A*), including TNFRSF10A, -B, and -D; TNFRSF8; TNFRSF11A; TNFRSF1B; and TNFRSF4. These receptors represent 7 of the top 10 up-regulated proteins in the apoptotic signaling pathway among the three cell lines, especially for the prostate epithelial derived cells. To test whether the overexpression of these receptors in the MYC-expressing prostate cells has functional effects, we treated both the MYC-overexpressing cells and their isogenic controls with the soluble agonist, TRAIL. Indeed, for the PrEC-LHS (Fig. 5*B*) and RWPE-1 cells (Fig. 5*C*) the MYC-overexpressing cells showed greater than 10-fold increased sensitivity by TRAIL-induced apoptosis. The sensitivity of the

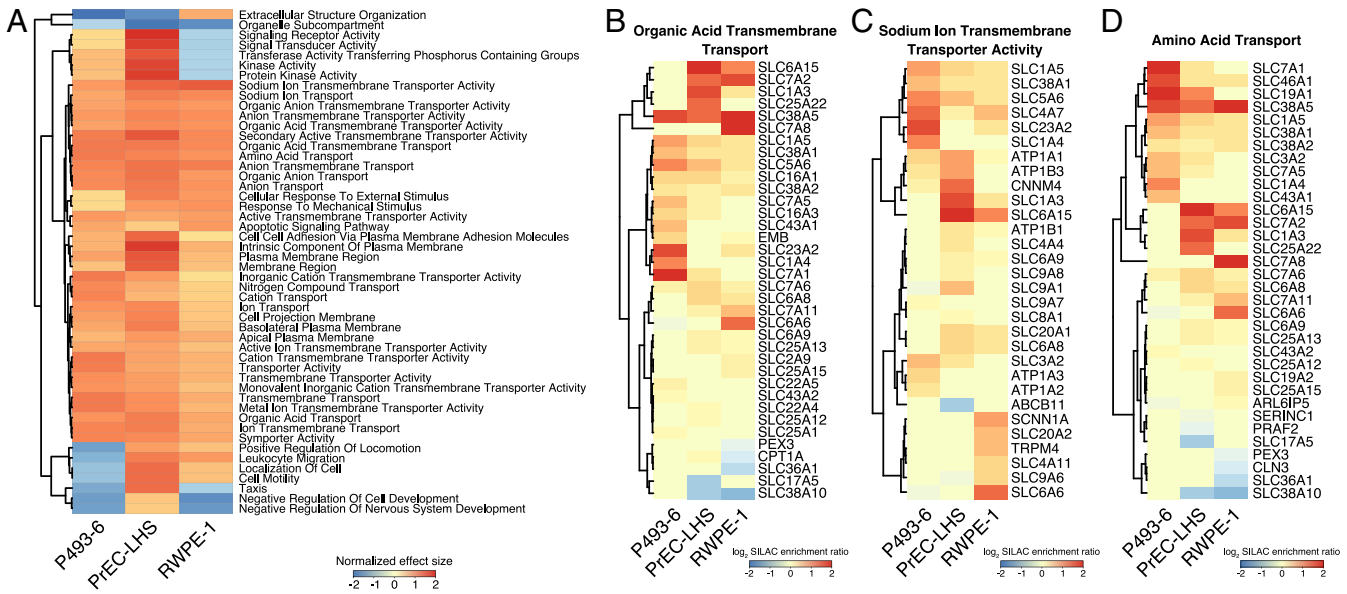

Fig. 3. Functional similarities revealed by GSEA among the high- versus low-MYC surfaceomic datasets for the P493-6 B cells and the RWPE-1 and PrEC-LHS prostate cells. (*A*) Top 50 enriched gene sets identified by GSEA of the surfaceomic dataset using Gene Ontology terms show clustering among high- versus low-MYC surfaceomes for the three cell lines. Positive normalized effect size (up-regulation) is shown in red, and negative (down-regulation) normalized effect size is shown in blue. Proteins were preranked by median SILAC peptide ratio and GSEA was performed using MySigDB C5 GO gene set collection. (*B–D*) Surface proteins involved in organic acid transmembrane transport (GO: 1903825), sodium ion transmembrane transporter activity (GO: 0015081), and amino acid transport (GO: 0006865) that are up-regulated in the each of the three high- versus low-MYC surfaceomes with a distinct set of transporters.

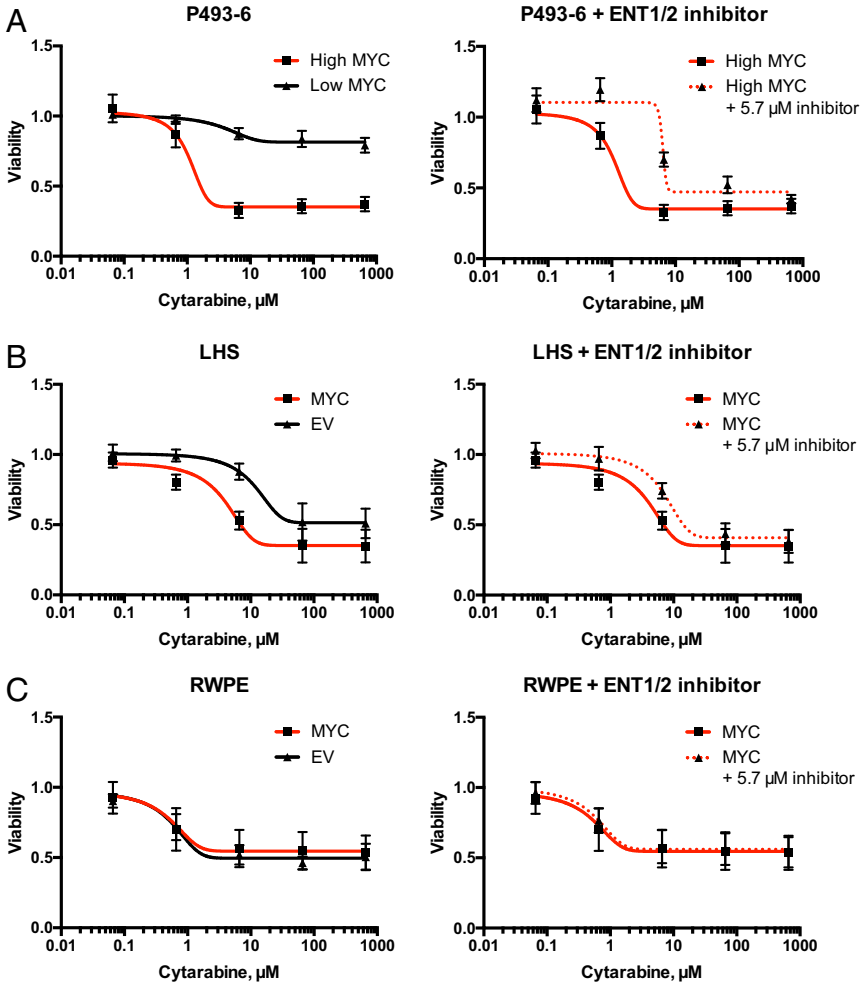

Fig. 4. Sensitivity of high- versus low-MYC expressing cells to the cytotoxic nucleotide, cytarabine (AraC) (*Right*) and protection afforded by ENT1/2 inhibitor S-(4-Nitrobenzyl)-6-thioinosine (*Left*). P493-6 B cells (*A*) and PrEC-LHS (*B*) and RWPE-1 (*C*) prostate cells expressing high MYC (red) were treated in duplicate with increasing concentrations of cytarabine (ranging up 650 nM) for 48 h and assayed for cell death using Cell Titer-Glo. MYC overexpression sensitizes P493-6 B-cells and PrEC-LHS cells to cytarabine which can be blocked by the ENT inhibitor, whereas the RWPE cells are extremely sensitive to cytarabine in both high- and low-MYC states.

MYC-overexpressing cells to TRAIL is comparable to that in some prostate cancer cell lines (40).

The PrEC-LHS cells have basal expression of MYC (*SI Appendix*, Fig. S5*A*). We sought to determine how this affected the basal cell surfaceome and so knocked down the basal MYC expression by threefold using CRISPR-mediated gene repression (CRISPRi) (41, 42) (*SI Appendix*, Fig. S5*A*) and determined the impact on the cell surfaceome between the untreated and the MYC knockdown cells. This had a mild bidirectional effect on cell surface protein expression among the 458 proteins detected (*SI Appendix*, Fig. S5*B*). This is not surprising because the starting MYC levels were low in the basal PrEC-LHS cells and thus the MYC knockdown had much smaller effects compared to those MYC-overexpressing cells seen earlier (Fig. 1*E*). This is also seen in the correlation plot of MYC overexpression versus knockdown in *SI Appendix*, Fig. S5*C* ($r = -0.5$). Interestingly, there were some targets that were especially sensitive, and in particular TNFSF10B was substantially suppressed by knockdown of MYC (*SI Appendix*, Fig. S5 *B* and *C*). We further validated the decreased expression of TNFSF10B using flow cytometry with a recombinant antibody to TNFRSF10B described below (*SI Appendix*, Fig. S5*D*).

The overexpression of TNFRSF10B impressed us as paradoxical as it would make cells susceptible to apoptosis in the presence of TRAIL (43, 44). In this same vein we also observed overexpression of NCR3LG1 (45, 46), a natural killer (NK) cell activating ligand, especially in the B cells and to a lesser degree in the prostate epithelial cells (Fig. 2*E*). This would make MYC-overexpressing cells more susceptible to NK killing and thus counter to their survival too.

Generation of Recombinant Antibodies to TNFRSF10B and NCR3LG1 to Further Validate Overexpression and Potential for Bispecific T Cell Engagement. To further validate our surface proteomics results we set out to generate recombinant and renewable antibodies to TNFRSF10B and NCR3LG1. We employed an antigen expression and Fab-phage display platform that has previously been used to produce high-quality recombinant antibodies to more than 500 human proteins (47) and more recently the ectodomains of surface proteins that we discovered are overexpressed by KRAS (48) (*SI Appendix*, Fig. S6). After four rounds of selection, individual phage clones were evaluated by ELISA and tested for high-affinity binding to the target ectodomain but not to Fc (*SI Appendix*, Fig. S7*A*). Clones passing this test were sequenced to bin into unique clones and analyzed for kinetic

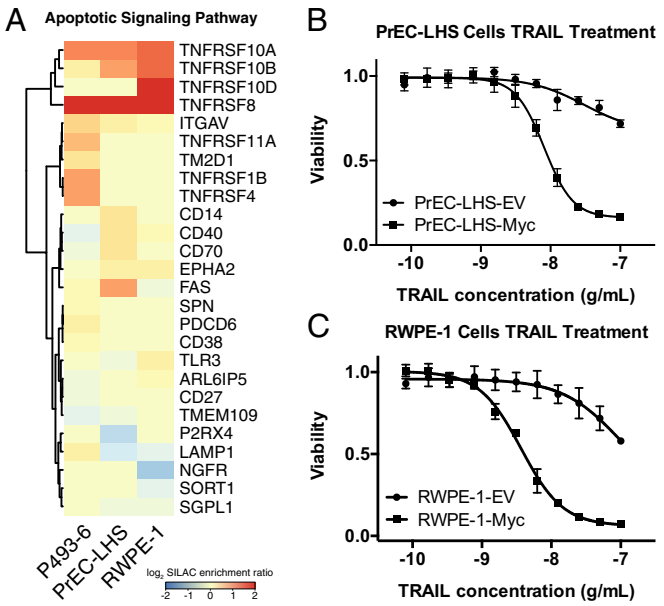

Fig. 5. Some prominent members of the apoptotic signaling pathways are generally up-regulated in high-MYC conditions and sensitize cells to TRAIL-induced apoptosis. (*A*) Proteins involved in apoptotic signaling pathways (GO: 0097190), including TNFRSF10A, TNFRSF10B, and TNFRSF8, are up-regulated in each of the three high- versus low-MYC surfaceomes. (*B* and *C*) PrEC-LHS and RWPE-1 cells in high- and low-MYC states were treated with recombinant TRAIL. MYC-overexpressing PrEC-LHS and RWPE-1 cells show much higher sensitivity to TRAIL-induced apoptosis.

and equilibrium binding properties by biolayer interferometry (*SI Appendix*, Figs. S7*B* and S8). Data are shown for two of the high-affinity Fabs obtained for TNFRSF10B and NCR3LG1 with dissociation constant values of 9.6 and 0.3 nM, respectively. We further validated the binding specificity on cells using CRISPRi knockdown cells (*SI Appendix*, Fig. S7*C*). We observed reduction in binding in the NCR3LG1 and TNFRSF10B knockdown cell lines relative to the isotype control as assessed by flow cytometry. These data validate that these high-affinity antibodies are specific for their target proteins on cells.

We next tested the ability of the antibodies to detect the overexpression of their respective target on the MYC overexpression cell lines relative to the low-MYC control cell lines. We first tested the anti-TNFRSF10B recombinant biotinylated Fab and found higher cell binding in both the high-MYC PrEC-LHS and high-MYC RWPE-1 cells (Fig. 6*A*) relative to the low-MYC isogenic cell controls. This further validates the mass spectrometry data showing similar increases in expression of TNFRSF10B on the high-MYC cells. We then cloned the anti-TNFRSF10B Fab into a BiTE format (49–51) by fusing the well-established anti-CD3 scFv (52, 53) to the C terminus of Fab heavy chain containing a His6-tag for purification. The anti-TNFRSF10B-BiTE was tested for T cell activation by coculturing low- or high-MYC cell lines with engineered Jurkat T cells containing an NFAT-GFP reporter (54). Indeed, the high-MYC cells showed significantly greater T cell activation than the low-MYC cells at 0.1 nM concentration of anti-TNFRSF10B-BiTE (Fig. 6*B*).

Using the same experimental platform as above we tested our high-affinity antibodies to NCR3LG1 for binding and T cell activation to high- and low-MYC cells (Fig. 7). Using the anti-NCR3LG1 recombinant biotinylated Fab, we were able to observe higher binding signal to high-MYC PrEC-LHS and high-MYC RWPE-1 cells relative to the low-MYC isogenic controls (Fig. 7*A*). The mass spectrometry data showed an almost eightfold increase in expression of NCR3LG1 in the high-MYC P493-6 cells (Figs. 1*B* and 2*E*). In addition to the high-MYC P493-6 cells, we examined the surface NCR3LG1 expression of two Burkitt's lymphoma cell lines, Raji (55) and Ramos (56) cells, known to have high levels of MYC and one low-MYC EBV-immortalized B cell line from a healthy doner (57) by anti-NCR3LG1 Fab staining (Fig. 7*C*). Indeed, all of the high-MYC cell lines showed up to fivefold higher levels of staining relative to the low-MYC EBV-immortalized B cells. We further constructed an anti-NCR3LG1-BiTE and found it activated Jurkat much better when mixed with the high-MYC PrEC-LHS and RWPE prostate cells relative to the low-MYC isogenic controls (Fig. 7*B*). We expanded the study to the P493-6, Raji, and Ramos cells compared to the low-MYC B cells. The anti-NCR3LG1-BiTE activation assay in the high-MYC B cells showed significant activation (Fig. 7*D*) that was about threefold higher than in the low-MYC controls. Collectively, the recombinant antibody studies corroborate that these targets are overexpressed in these cell lines and amenable to targeted killing using BiTE technology.

Discussion

MYC is one of the most dominant transcription factors affecting expression of 10 to 15% of genes and is often highly up-regulated in B cell and prostate cancer cells as well as others (58). To systematically understand how MYC overexpression affects the cell surfaceome based on cell types in a cell autologous fashion, we took a reductionist approach where we generated or employed isogenic cell lines having either low or high levels of MYC expression. These isogenic models are certainly oversimplified because no single cell type or context can recapitulate real tumors. However, we believe this is an important and pragmatic approach to investigate the surface proteome regulated by MYC

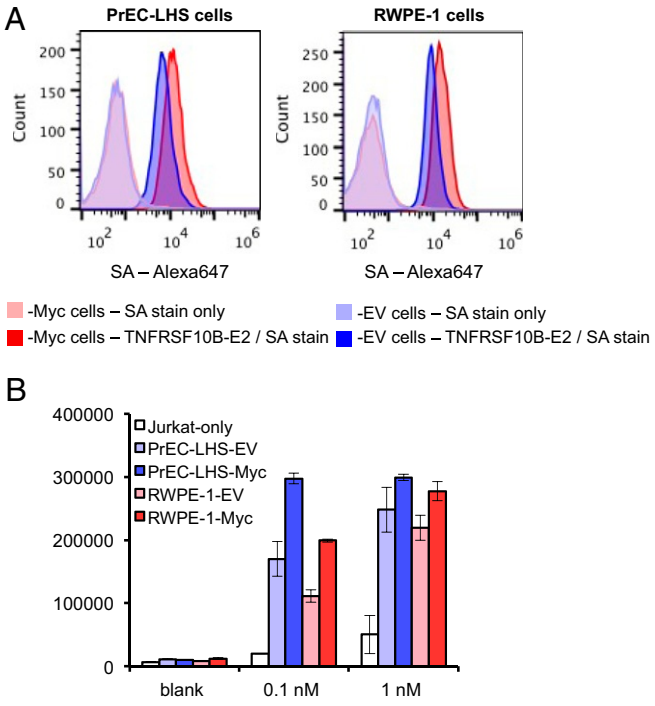

Fig. 6. Anti-TNFRSF10B antibody E2 shows preferred binding to PrEC-LHS and RWPE-1 cells with MYC overexpression. (*A*) The TNFRSF10B BiTE activates Jurkat cells significantly better in cells with MYC overexpression than in cells without MYC overexpression when treated with 0.1 nM BiTE. (*B*) Treatment with the TNFRSF10B BiTE alone resulted in no significant T cell activation.

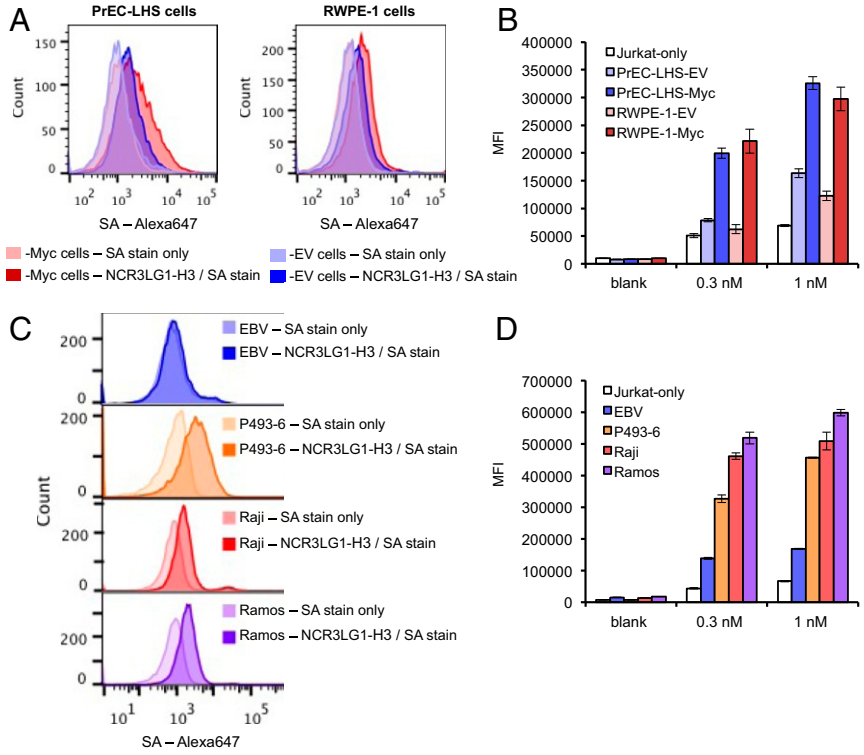

Fig. 7. Anti-NCR3LG1 antibody H3 shows preferred binding to high-MYC cell lines and the NCR3LG1 BiTE activates Jurkat cells when coculturing with high-MYC cells. (*A*) NCR3LG1 antibody H3 shows higher binding to PrEC-LHS and RWPE-1 cells with MYC overexpression. (*B*) The NCR3LG1 BiTE activates Jurkat cells at 0.3 and 1 nM when coculturing with PrEC-LHS and RWPE-1 cells overexpressing MYC while keeping the activation of Jurkat cells to a minimum when coculturing with PrEC-LHS and RWPE-1 cells without MYC overexpression. (*C*) NCR3LG1 antibody H3 shows strong binding to high-MYC P493-6 (orange), Raji (red), and Ramos (purple), but no visible binding to a low-MYC EBV immortalized B cell line. (*D*) NCR3LG1 BiTE activates Jurkat cells at 0.3 and 1 nM when coculturing with high-MYC P493-6, Raji, and Ramos cells while keeping the activation of Jurkat cells to a minimum when coculturing with low-MYC EBV-immortalized B cells.

overexpression in a highly controlled setting where one can obtain pure and reproducible samples compared to more complex primary tumors.

The surfaceomics data show dramatic changes where MYC overexpression induces 2- to 10-fold changes for 20 to 30% of the total 500 to 800 observed surface proteins. We realize our sampling is incomplete because we will miss nonglycosylated proteins and ones of low abundance. Nonetheless we estimate we would have sampled up to one-third of the total surfaceome based on the expectation that there are a total of 4,000 annotated membrane protein genes and that about half of the genome is expressed at any given time (31, 32). Even though Myc overexpression has been shown to amplify gene transcription globally (amplifier of transcription) (59, 60), it is possible that that global increase of gene transcription might not strongly correlate at the protein level. We have observed poor correlation between surfaceome and RNA sequencing data in our previous studies on membrane proteins (48, 61, 62). The changes we observe are remarkably symmetric and bidirectional, reflecting a movement from one state to another. We find there are corresponding phenotypic consequences, such as increased proliferation rate that correlated with MYC overexpression in B cells. While no significant alteration of cell growth by MYC overexpression is observed in PrEC-LHS and RWPE-1 cell lines, morphological changes are observed for MYC overexpression. The precise changes we see are highly cell type dependent as more than half of the expression changes vary among the three cell lines. Even the two prostate epithelial cell lines differed from each other almost as much as they differed from the B cell line, individually. This may not be surprising given that MYC drives so many genes. Others have found MYC induces expression of PD-L1 and CD47 in T cell acute lymphoblastic leukemia (TALL) (6). We did detect these two proteins but did not observe them systematically altered by MYC overexpression (*SI Appendix*, Fig. S9). This could be due to the differences between the cell lines here and the TALL cell line used previously. For the prostate cell line comparison, a recent systematic analysis of cell surface proteomes from a variety of prostate cancer cell lines coupled to previously published transcriptome expression analysis identified geneset ion transmembrane transport to be up-regulated in the neuroendocrine prostate cancer (NEPC) subtype (63, 64). NEPC is known to harbor MYC amplification and is consistent with our observation of geneset enrichment of transmembrane transport.

Despite the differences in individual protein expression there is remarkable coherence in protein functions. This highlights the functional redundancy among the up-regulated proteins and the functional convergence of MYC oncogenesis in different cellular contexts. The most dominant class that is systematically up-regulated is the solute, metabolite, and metal ion carriers (Fig. 3*A*). Of the 365 targets seen up-regulated by twofold or greater in at least one of the Myc-overexpression cell lines (Fig. 2*B*), 82 are connected to transmembrane transport (GO: 0055085, 199 proteins identified with this annotation in the current study). Of the roughly 4,000 genes encoding membrane proteins, there are 415 annotated solute carrier proteins (31, 32). Thus, while solute carrier class genes represent about 10% of the genes encoding the surfaceome, roughly a quarter of the up-regulated proteins induced by MYC overexpression are in this class. MYC is known to drive proliferation and has its

greatest effect on increasing translation, an anabolic process with tremendous nutrient requirement (7, 26). We have recently performed surfaceomic studies on a common isogenic breast epithelial cell line containing oncogenes such as oncogenic KRAS, EGFR, HER2, BRAF, MEK, and Akt that drive proliferation through the MAPK or Akt pathways. In these studies we observed a total of 375 proteins upregulated and only 44 annotated with transmembrane transport activity (GO: 0055085), representing 11.7% (62). Thus, compared to other oncogenes, MYC seems to have a particularly strong and differential effect in promoting the solute carriers.

There are at least 20 targets that are commonly up-regulated in all three cell lines, and 7 belong to the solute carrier family including SLC1A5, SLC29A1, SLC30A1, SLC43A3, SLC38A5, SLC29A2, and SLC5A6. Two of these, SLC29A1 and SLC29A2, also known as ENT1 and ENT2, are nucleoside transporters that have been found to be overexpressed in colon cancer. It is not surprising to find that 6 of these 7 SLC transporters do not appear to be essential to most cell lines, whereas 170 of 808 cell lines in CRISPR screens (CRISPR [Avana] Public 20Q4) and 5 of 710 cell lines in RNAi screens (combined RNAi) are found to be dependent on SLC1A5 (*SI Appendix*, Fig. S10) (65–67). MYC regulation of these transporters in combination with dysregulation of efflux pumps determines overall sensitivity vs. resistance to toxic nucleosides like cytarabine (68, 69). We found the MYC-induced overexpression of ENT1/2 leads to increased sensitivity to cytarabine for at least two of the three cell lines, the P493-6 B cells and the PrEC-LHS prostate cells, but that RWPE cells were highly sensitive independent of MYC expression and did not depend on ENT1/2. It is possible that cytarabine is getting into RWPE cells via another transporter and/or that these cells lack ABC transporters that efflux the drug (70, 71). MYC levels have been correlated to both up- and down-regulation of ABC efflux pumps (71). ABCC4 has been demonstrated to participate in cytarabine efflux, and likely other members of the ABCC family also mediate its export (72). Three of the other SLCs (SLC1A5, SLC38A5, and SLC43A3) also found commonly up-regulated on the three cell lines are organic acid and amino acid transporters. While SLC43A3 is an orphan transporter whose function is less known (73), SLC1A5 and SLC38A5 are glutamine transporters that are often up-regulated in cancers for enhanced glutaminolysis (74–77). The last two are SLC5A6, a sodium/vitamin transporter (78), and SLC30A1, a Zn2+ transporter known to be highly expressed in nonsmall cell lung cancer (79). The three cell lines used in this study are not suitable for elucidating the dependency on SLC transporters for Myc-driven cancer cell growth because the growth of both PrEC-LHS and RWPE-1 is not dependent on Myc overexpression and P493-6 is an engineered cell line with Myc placing under an artificial tet-off system. Nonetheless, Yue et al. (80) found that SLC7A5 loss by RNA interference resulted in diminished Myc expression and lower growth for Daudi cells consistent with its importance. Our data highlight the possibility of using cytotoxic metabolites to target the up-regulated transporters, recognizing that the balance of transport and efflux can be complex and pleotropic with redundant functions.

Another class of proteins that are systematically up-regulated is TNF receptor superfamily members, including TNFRSF10A, -B, and -D; TNFRSF8; TNFRSF11A; TNFRSF1B; and TNFRSF4; which paradoxically sensitize cells to killing by TNF family members. Other studies have shown that MYC sensitizes cells to apoptosis and to TRAIL (43, 44). Indeed, we find that the MYC overexpression in the prostate epithelial cells was 10- to 100-fold more sensitive to TRAIL killing than the non-MYC overexpression control. In particular, TNFRSF10B was highly overexpressed and common in all three surfaceomic datasets. It is not clear whether enhanced TNFRSF10B transcription upon MYC overexpression is responsible for this finding. It is also possible that differential protein degradation and trafficking are responsible for higher TNFRSF10B abundance on the cell surface upon MYC overexpression. We found that the whole-cell TNFRSF10B levels in PrEC-LHS-Myc and RWPE-1-Myc cells are unchanged or decreased, respectively, in comparison to their corresponding EV cells (*SI Appendix*, Fig. S11). A recombinant antibody we generated to the ectodomain of TNFRSF10B further demonstrated overexpression of TNFRSF10B in the Myc-overexpressed cell lines. Moreover, the antibody could activate T cells in a BiTE format justifying further preclinical investigation of this target antibody. In this same vein we identified the NK activating ligand, also called B7-H6, for binding NK30p on NK cells (45, 81). NCR3LG1 was commonly up-regulated on all three MYC-overexpression cell lines. The high-affinity recombinant antibodies to NCR3LG1 we produced showed increased binding to cells overexpressing MYC, further validating the surfaceomics data. Moreover, an anti-NCR3LG1 BiTE construct was found to activate T cells to a greater degree for the MYC-overexpression cells as well as Raji and Ramos cells also found to overexpress MYC and NCR3LG1.

The expression of these TNF receptor family members as well as the NK cell activating ligand is paradoxical to cell survival but there are other examples. It has long been known that constitutive expression of MYC suppresses cell cycle arrest and accelerates intrinsic apoptosis often in a p53-dependent fashion through the mitochondria by elevation of proapoptotic BH3 family members (82). More recently it has been discovered that MYC expression can induce apoptosis through the extrinsic pathway, such as the FAS receptor (83). Others have shown MYC can up-regulate the DR5 receptor for TRAIL (44). To rationalize these findings it has been proposed that MYC overexpression leads to sensitization to apoptosis that may serve as a cell surface fail-safe mechanism like p53 to remove cells with inappropriate MYC activation prior to complete development of the cancer phenotype (43). Our findings are consistent with these published reports.

In summary, we believe the surfaceomics datasets comparing low-MYC and high-MYC expressing cells provide a useful resource for understanding how MYC dramatically remodels the surfaceome in a cell autologous fashion. This work adds to our understanding of MYC biology and provides focused sets of surface targets and combinations to validate in more complex settings. These studies provide a useful data resource for generating recombinant antibodies to further validate potential cancer drug targets.

Materials and Methods

Cell Line Generation for Surfaceomic Experiments. Parental P493-6, RWPE-1, and PrEC-LHS were a gift from Michael J. Evans at University of California, San Francisco. The lentiviral transfer plasmid pCDH-puro-cMyc was purchased from Addgene (Addgene: 46970) (84). pCDH-puro-cMyc was modified to create pCDH-zeo-cMyc in which the puromycin resistance gene was replaced by a zeocin resistance gene (Ble). The Myc gene in pCDH-zeo-cMyc was then replaced by a piece of short decoy sequence (ATCGATCGATCGATCG) to create the empty vector plasmid pCDH-zeo-EV. RWPE-1-EV and PrEC-LHS-EV were generated by lentiviral transduction of pCDH-zeo-EV into the parental RWPE-1 and PrEC-LHS cells, respectively. RWPE-1-Myc and PrEC-LHS-Myc were generated by lentiviral transduction of pCDH-zeo-Myc into the parental RWPE-1 and PrEC-LHS cells, respectively. After transduction, cells were allowed to recover for 2 d prior to zeocin resistance selection (200 μg/mL) for 1 wk. P493-6 and PrEC-LHS cells were grown in RPMI 1640 media (GE Healthcare Life Sciences) supplemented with 10% fetal bovine serum. RWPE-1 cells were grown in Keratinocyte Serum Free Medium (Gibco). The transduced stable cell lines are maintained in media supplemented with zeocin (50 μg/mL).

SILAC, ReDiMe Labeling, and CSC. P493-6 cells were cultured in RPMI 1640 SILAC media (Gibco) containing L-[$^{13}C_6$,$^{15}N_2$] lysine and L-[$^{13}C_6$,$^{15}N_4$] arginine (heavy label; Cambridge Isotope Laboratories) or L-[$^{12}C_6$,$^{14}N_2$] lysine and L-[$^{12}C_6$,$^{14}N_4$] arginine (light label) for five passages to ensure full incorporation of the isotope labeling on cells. The heavy and light P493-6 cells were used for generating high-Myc and low-Myc P493-6 cells by culturing without or with 100 ng/mL tetracycline treatment, respectively. 20×10^6 heavy or light P493-6 cells were harvested and mixed at 1:1 cell count ratio and subjected to the CSC protocol. The RWPE-1 and PrEC-LHS cell lines were cultured with regular media and 20×10^6 cells were harvested at 80% confluence and subjected to the CSC protocol. We employed the CSC labeling technique that captures surface glycoproteins by mild periodate treatment followed by reaction with biotin-hydrazide to install biotin handles on glycan units for the subsequent purification of the surface glycoproteins (85). Briefly, after cell lysis the cell surface glycoproteins were enriched by binding to neutravidin beads, followed by on-bead tryptic digestion, and recovery of the N-linked tryptic peptide by hydrolysis of the N-glycan bond with PNGase treatment (48). The samples for RWPE-1 and PrEC-LHS cells went through an additional step to introduce the heavy and light isotopic labels by ReDiMe (38) with a modified protocol. Briefly, after cell lysis and binding to neutravidin beads, the beads were washed with radioimmunoprecipitation assay buffer, high-salt buffer (1 M NaCl, phosphate-buffered saline (PBS) pH 7.5), and urea buffer (2 M urea, PBS pH 7.5). The samples were reduced on-bead with 5 mM tris(2-carboxyethyl)phosphine at 55 °C for 30 min and alkylated with 10 mM iodoacetamide at room temperature for 30 min. The beads were then washed with H_2O and urea buffer (2 M urea, 100 mM triethylammonium bicarbonate). The samples were then digested on-bead by trypsin in urea buffer (2 M urea, 100 mM triethylammonium bicarbonate). To each digested sample (per 200 μL), add 8 μL of 4% formaldehyde (light label) or 8 μL of 4% formaldehyde-^{13}C, d_2 solution (heavy label; Sigma-Aldrich) and 8 μL of 0.6 M sodium cyanoborohydride. The samples were incubated for 1 h at room temperature while shaking. To quench the reaction, add 32 μL of 1% NH_4OH followed by 16 μL of formic acid. The PNGase cleaved peptides and tryptic peptides were then analyzed separately with bottom–up proteomics with data-dependent acquisition as previously described (48, 61, 62, 86). Results were filtered for cell surface proteins, combined, and quantified by Skyline (87). The proteomics data were deposited in MassIVE (http://massive.ucsd.edu) with the ProteomeXchange deposition number PXD020799 and MassIVE identifier MSV000085930.

Vector Design and Construction. The vector used to express the ECDs of TNFRSF10B and NCR3LG1 was generated by Gibson cloning and adapted from the pFUSE-hIgG1-Fc (InvivoGen) vector as previously described (48). We used a previously described vector for expression of Fabs and BiTEs (47, 48). Previously described vectors were used for CRISPRi experiments (42, 48). Individual sgRNAs TNFRSF10B (TNFRSF10B_+_22926121.23-P1P2): GGGCAAGACGCACCAGTCGT; NCR3LG1 (NCR3LG1_-_17373307.23-P1P2): GGTGGGGCTGGTCACGCGCC; MYC (MYC_+_128747801.23-P1P2): GGGGCGCGCGTTCAGAGCGT were cloned into a pU6 lentiviral vector (Addgene: 46914) and dCas9-BFP-KRAB was expressed from a pHR-SFFV lentiviral vector (Addgene: 46911) (42).

Cell Line Generation for CRISPRi Experiments. PrEC-LHS-dCas9-KRAB cells were obtained by lentiviral transduction of dCas9-BFP-KRAB into the parental PrEC-LHS cells. Transduced cells were allowed to recover for 2 d prior to two rounds of cell sorting based on BFP expression. PrEC-LHS-dCas9-KRAB cells expressing sgRNA constructs are obtained by lentiviral transduction by sgRNA plasmids into the PrEC-LHS-dCas9-KRAB cells. Transduced cells were allowed to recover for 2 d prior to cell sorting based on GFP expression.

Phage Panning Procedure and Phage ELISA. The ectodomains of the type I single-pass TNFRSF10B and NCR3LG1 were expressed as Fc-fusion proteins in expiHEK293T cells to facilitate secretion and glycosylation and further engineered to perform site-specific C-terminal biotinylation in cells, as described in Martinko et al. (48). The biotinylated Fc-fusion proteins were purified by protein A affinity chromatography and immobilized on magnetic beads containing bound streptavidin. We conducted four rounds of "catch and release" selections with a well-validated and high-diversity Fab-phage library (3×10^9 variants) containing synthetic variant CDRs for CDRL3, CDRH1, CDRH2, and CDRH3 (88). The Fc-domain alone was used for negative selection to remove any unwanted Fc-binding antibodies. Phage ELISAs were conducted using a previously described protocol. Ninety-six-well Maxisorp plates were coated with NeutrAvidin (10 mg/mL) overnight at 4 °C and were blocked with bovine serum albumin (BSA) (2% wt/vol) for 1 h at 20 °C. A total of 20 nM of biotinylated ECD-Fc-fusion or Fc-domain was captured on the NeutrAvidin-coated wells for 30 min followed by the addition of phage supernatants diluted 1:5 in ELISA buffer (PBS, pH 7.4, 0.05% Tween-20, 0.2% BSA) for 30 min. Phages that were bound to the plates were then detected using a horseradish peroxidase (HRP)-conjugated antiphage monoclonal antibody (GE Lifesciences).

Expression of Fabs and BiTEs. Avi-tagged Fabs and BiTEs (light-chain fused to an anti-CD3 scFv) were expressed following a previously described protocol (48). Briefly, *Escherichia coli* C43 (DE3) containing expression plasmids were grown in Terrific Broth supplemented with 1 mg/mL D-Biotin at 37 °C to OD_{600} of 0.6 to 0.8 and then Fab and BiTE expression was induced by the addition of 1 mM and 0.1 nM isopropyl β-D-1-thiogalactopyranoside, respectively. Incubation temperature was subsequently reduced to 30 °C and 20 °C, respectively, and the cultures were allowed to shake for 16 to 18 h. Cells were harvested and lysed by sonication and Fabs were purified by Protein A affinity chromatography and Ni-NTA chromatography, respectively.

Preparation of CRISPRi Cell Lines. HEK293T cells were transfected with sgRNA plasmids for TNFRSF10B and NCR3LG1 described previously (42) to generate viral particles. Two days after infection, PrEC-LHS and RWPE-1 cells were treated with puromycin for 3 d to select for sgRNA expression before being taken to medium without puromycin for 2 d of recovery.

BiTE assay. Jurkat NFAT-reporter cells were mixed with high-Myc or low-Myc cells at a ratio of 1:1. Bispecic T cell engaging antibody (BiTEs) (anti-TNFRSF10B-anti-CD3 or anti-NCR3LG1-anti-CD3) was diluted in medium and added to cell mixtures at a final concentration of 0.3 or 1 nM. A total of 1 nM anti-TNFRSF10B or anti-NCR3LG1 Fab is used as a blank control. After 20 h incubation at 37 °C, cells were pelleted by centrifugation. NFAT-dependent GFP reporter expression was quantified by flow cytometry using a CytoFLEX (Beckman Coulter).

Cytarabine Cytotoxicity Assay. P493-6 cells expressing low (treated with 1 μg/mL tetracycline for 36 h) or high Myc, PrEC-LHS cells expressing EV or high Myc, and RWPE cells expressing EV or high Myc were seeded in 96-well plates at 10,000 cells per well. Cells were treated with doses of 0 to 656 μM cytarabine (Sigma), solubilized in dimethylsulfoxide (DMSO), and added to cells at final concentration of 0.05% DMSO. To demonstrate the mechanism of sensitivity, a separate set of cytotoxic nucleoside dose titrations was cotreated with 5.7 μM S-(4-Nitrobenzyl)-6-thioinosine (Sigma), a specific ENT1/2 inhibitor. After 48 h cell viability was assayed by Cell Titer-Glo (Promega) per manufacturer protocol.

TRAIL-Induced Apoptosis Assay. PrEC-LHS and RWPE-1 cells with or without Myc overexpression were grown to 80% confluency and lifted by versene solution. Cells were seeded to 50% confluency to allow the cells to recover for 1 d before adding recombinant TRAIL (R&D Systems) and incubating at 37 °C for 18 h. The cell viability is then obtained by WST-8 assay (Cayman Chemical Company) per manufacturer protocol.

Data Availability. All proteomics datasets are deposited in MassIVE (http://massive.ucsd.edu) with the ProteomeXchange deposition number PXD020799 and MassIVE identifier MSV000085930.

ACKNOWLEDGMENTS. We thank Professor Michael Evans at University of California, San Francisco (UCSF) for kindly providing cell lines and Professor Michael Evans and Professor Davide Ruggero for the helpful discussions. We thank Arthur Weiss (UCSF) and Theresa Kadlecek (UCSF) for providing the NFAT-dependent GFP reporter Jurkat cell line. We thank Dr. Xin Zhou and other members of the Wells laboratory for useful discussions. K.K.L. was supported in part by the Canadian Institutes of Health Research. Much of this work was supported by funding from UCSF Prostate Cancer Program New Directions Awards, National Cancer Institute P41CA196276, and the Harry and Dianna Hind Professorship in Pharmaceutical Sciences (J.A.W.).

1. F. Lorenzin *et al.*, Different promoter affinities account for specificity in MYC-dependent gene regulation. *eLife* **5**, e15161 (2016).
2. M. Muhar *et al.*, SLAM-seq defines direct gene-regulatory functions of the BRD4-MYC axis. *Science* **360**, 800–805 (2018).
3. D. Horiuchi *et al.*, PIM1 kinase inhibition as a targeted therapy against triple-negative breast tumors with elevated MYC expression. *Nat. Med.* **22**, 1321–1329 (2016).
4. L. Soucek *et al.*, Modeling Myc inhibition as a cancer therapy. *Nature* **455**, 679–683 (2008).

5. L. E. Pascal *et al.*, Correlation of mRNA and protein levels: Cell type-specific gene expression of cluster designation antigens in the prostate. *BMC Genom.* **9**, 246 (2008).
6. S. C. Casey *et al.*, MYC regulates the antitumor immune response through CD47 and PD-L1. *Science* **352**, 227–231 (2016).
7. C. V. Dang, MYC on the path to cancer. *Cell* **149**, 22–35 (2012).
8. J. Liu, D. Levens, Making myc. *Curr. Top. Microbiol. Immunol.* **302**, 1–32 (2006).
9. H. Clevers, Wnt breakers in colon cancer. *Canc. Cell* **5**, 5–6 (2004).
10. R. Dalla-Favera *et al.*, Human c-myc onc gene is located on the region of chromosome 8 that is translocated in Burkitt lymphoma cells. *Proc. Natl. Acad. Sci. U.S.A.* **79**, 7824–7827 (1982).
11. R. Dalla-Favera *et al.*, The human onc gene c-myc: Structure, expression, and amplification in the human promyelocytic leukemia cell line HL-60. *Haematol. Blood Transfus.* **28**, 247–254 (1983).
12. R. Taub *et al.*, Translocation of the c-myc gene into the immunoglobulin heavy chain locus in human Burkitt lymphoma and murine plasmacytoma cells. *Proc. Natl. Acad. Sci. U.S.A.* **79**, 7837–7841 (1982).
13. M. Toyoshima *et al.*, Functional genomics identifies therapeutic targets for MYC-driven cancer. *Proc. Natl. Acad. Sci. U.S.A.* **109**, 9545–9550 (2012).
14. TCGAR Network *et al.*, The molecular taxonomy of primary prostate cancer. *Cell* **163**, 1011–1025 (2015).
15. C. M. Koh *et al.*, MYC and prostate cancer. *Genes Cancer* **1**, 617–628 (2010).
16. D. Hawksworth *et al.*, Overexpression of C-MYC oncogene in prostate cancer predicts biochemical recurrence. *Prostate Cancer Prostatic Dis.* **13**, 311–315 (2010).
17. B. S. Taylor *et al.*, Integrative genomic profiling of human prostate cancer. *Canc. Cell* **18**, 11–22 (2010).
18. D. A. Quigley *et al.*, Genomic hallmarks and structural variation in metastatic prostate cancer. *Cell* **174**, 758–769 e9 (2018).
19. A. Kumar *et al.*, Substantial interindividual and limited intraindividual genomic diversity among tumors from men with metastatic prostate cancer. *Nat. Med.* **22**, 369–378 (2016).
20. D. Robinson *et al.*, Integrative clinical genomics of advanced prostate cancer. *Cell* **162**, 454 (2015).
21. C. Sun *et al.*, TMPRSS2-ERG fusion, a common genomic alteration in prostate cancer activates C-MYC and abrogates prostate epithelial differentiation. *Oncogene* **27**, 5348–5353 (2008).
22. C. V. Dang *et al.*, The c-Myc target gene network. *Semin. Canc. Biol.* **16**, 253–264 (2006).
23. C. Arvanitis, D. W. Felsher, Conditional transgenic models define how MYC initiates and maintains tumorigenesis. *Semin. Canc. Biol.* **16**, 313–317 (2006).
24. C. M. Shachaf, D. W. Felsher, Tumor dormancy and MYC inactivation: Pushing cancer to the brink of normalcy. *Cancer Res.* **65**, 4471–4474 (2005).
25. H. Chen, H. Liu, G. Qing, Targeting oncogenic Myc as a strategy for cancer treatment. *Signal Transduct. Target. Ther.* **3**, 5 (2018).
26. L. Soucek, G. I. Evan, The ups and downs of Myc biology. *Curr. Opin. Genet. Dev.* **20**, 91–95 (2010).
27. I. A. Asangani *et al.*, Therapeutic targeting of BET bromodomain proteins in castration-resistant prostate cancer. *Nature* **510**, 278–282 (2014).
28. A. Wyce *et al.*, Inhibition of BET bromodomain proteins as a therapeutic approach in prostate cancer. *Oncotarget* **4**, 2419–2429 (2013).
29. F. Brasó-Maristany *et al.*, PIM1 kinase regulates cell death, tumor growth and chemotherapy response in triple-negative breast cancer. *Nat. Med.* **22**, 1303–1313 (2016).
30. A. N. Kirschner *et al.*, PIM kinase inhibitor AZD1208 for treatment of MYC-driven prostate cancer. *J. Natl. Cancer Inst.* **107**, dju407 (2014).
31. R. Gonzalez *et al.*, Screening the mammalian extracellular proteome for regulators of embryonic human stem cell pluripotency. *Proc. Natl. Acad. Sci. U.S.A.* **107**, 3552–3557 (2010).
32. E. Wallin, G. von Heijne, Genome-wide analysis of integral membrane proteins from eubacterial, archaean, and eukaryotic organisms. *Protein Sci.* **7**, 1029–1038 (1998).
33. B. Wollscheid *et al.*, Mass-spectrometric identification and relative quantification of N-linked cell surface glycoproteins. *Nat. Biotechnol.* **27**, 378–386 (2009).
34. A. Pajic *et al.*, Cell cycle activation by c-myc in a Burkitt lymphoma model cell line. *Int. J. Canc.* **87**, 787–793 (2000).
35. S. E. Ong *et al.*, Stable isotope labeling by amino acids in cell culture, SILAC, as a simple and accurate approach to expression proteomics. *Mol. Cell. Proteomics* **1**, 376–386 (2002).
36. R. Berger *et al.*, Androgen-induced differentiation and tumorigenicity of human prostate epithelial cells. *Canc. Res.* **64**, 8867–8875 (2004).
37. D. Bello, M. M. Webber, H. K. Kleinman, D. D. Wartinger, J. S. Rhim, Androgen responsive adult human prostatic epithelial cell lines immortalized by human papillomavirus 18. *Carcinogenesis* **18**, 1215–1223 (1997).
38. A. C. Tolonen, W. Haas, Quantitative proteomics using reductive dimethylation for stable isotope labeling. *JoVE* **89**, e51416 (2014).
39. P. Macanas-Pirard *et al.*, Resistance of leukemia cells to cytarabine chemotherapy is mediated by bone marrow stroma, involves cell-surface equilibrative nucleoside transporter-1 removal and correlates with patient outcome. *Oncotarget* **8**, 23073–23086 (2017).
40. X. Chen *et al.*, Constitutively active Akt is an important regulator of TRAIL sensitivity in prostate cancer. *Oncogene* **20**, 6073–6083 (2001).
41. L. A. Gilbert *et al.*, CRISPR-mediated modular RNA-guided regulation of transcription in eukaryotes. *Cell* **154**, 442–451 (2013).
42. L. A. Gilbert *et al.*, Genome-scale CRISPR-mediated control of gene repression and activation. *Cell* **159**, 647–661 (2014).
43. B. Hoffman, D. A. Liebermann, Apoptotic signaling by c-MYC. *Oncogene* **27**, 6462–6472 (2008).
44. Y. Wang *et al.*, Synthetic lethal targeting of MYC by activation of the DR5 death receptor pathway. *Canc. Cell* **5**, 501–512 (2004).
45. C. S. Brandt *et al.*, The B7 family member B7-H6 is a tumor cell ligand for the activating natural killer cell receptor NKp30 in humans. *J. Exp. Med.* **206**, 1495–1503 (2009).
46. S. Textor *et al.*, The proto-oncogene Myc drives expression of the NK cell-activating NKp30 ligand B7-H6 in tumor cells. *OncoImmunology* **5**, e1116674 (2016).
47. M. Hornsby *et al.*, A high through-put platform for recombinant antibodies to folded proteins. *Mol. Cell. Proteomics* **14**, 2833–2847 (2015).
48. A. J. Martinko *et al.*, Targeting RAS-driven human cancer cells with antibodies to upregulated and essential cell-surface proteins. *eLife* **7**, e31098 (2018).
49. J. Wu, J. Fu, M. Zhang, D. Liu, Blinatumomab, a bispecific T cell engager (BiTE) antibody against CD19/CD3 for refractory acute lymphoid leukemia. *J. Hematol. Oncol.* **8**, 104 (2015).
50. X. Wu *et al.*, Fab-based bispecific antibody formats with robust biophysical properties and biological activity. *mAbs* **7**, 470–482 (2015).
51. T. Yuraszeck, S. Kasichayanula, J. E. Benjamin, Translation and clinical development of bispecific T-cell engaging antibodies for cancer treatment. *Clin. Pharmacol. Ther.* **101**, 634–645 (2017).
52. M. Compte *et al.*, Functional comparison of single-chain and two-chain anti-CD3-based bispecific antibodies in gene immunotherapy applications. *OncoImmunology* **3**, e28810 (2014).
53. A. Salmeron, F. Sanchez-Madrid, M. A. Ursa, M. Fresno, B. Alarcon, A conformational epitope expressed upon association of CD3-epsilon with either CD3-delta or CD3-gamma is the main target for recognition by anti-CD3 monoclonal antibodies. *J. Immunol.* **147**, 3047–3052 (1991).
54. E. Hooijberg, A. Q. Bakker, J. J. Ruizendaal, H. Spits, NFAT-controlled expression of GFP permits visualization and isolation of antigen-stimulated primary human T cells. *Blood* **96**, 459–466 (2000).
55. T. H. Rabbitts, A. Forster, P. Hamlyn, R. Baer, Effect of somatic mutation within translocated c-myc genes in Burkitt's lymphoma. *Nature* **309**, 592–597 (1984).
56. J. Fogh, Human tumor lines for cancer research. *Cancer Invest.* **4**, 157–184 (1986).
57. G. Tosato, J. I. Cohen, Generation of Epstein-Barr virus (EBV)-immortalized B cell lines. *Curr. Protoc. Immunol.*, 7.22.1–7.22.4 (2007).
58. P. S. Knoepfler, Myc goes global: New tricks for an old oncogene. *Cancer Res.* **67**, 5061–5063 (2007).
59. C. Y. Lin *et al.*, Transcriptional amplification in tumor cells with elevated c-Myc. *Cell* **151**, 56–67 (2012).
60. Z. Nie *et al.*, C-Myc is a universal amplifier of expressed genes in lymphocytes and embryonic stem cells. *Cell* **151**, 68–79 (2012).
61. K. K. Leung *et al.*, Multiomics of azacitidine-treated AML cells reveals variable and convergent targets that remodel the cell-surface proteome. *Proc. Natl. Acad. Sci. U.S.A.* **116**, 695–700 (2019).
62. K. K. Leung *et al.*, Broad and thematic remodeling of the surfaceome and glycoproteome on isogenic cells transformed with driving proliferative oncogenes. *Proc. Natl. Acad. Sci. U.S.A.* **117**, 7764–7775 (2020).
63. H. Beltran *et al.*, Divergent clonal evolution of castration-resistant neuroendocrine prostate cancer. *Nat. Med.* **22**, 298–305 (2016).
64. J. K. Lee *et al.*, Systemic surfaceome profiling identifies target antigens for immune-based therapy in subtypes of advanced prostate cancer. *Proc. Natl. Acad. Sci. U.S.A.* **115**, E4473–E4482 (2018).
65. R. M. Meyers *et al.*, Computational correction of copy number effect improves specificity of CRISPR-Cas9 essentiality screens in cancer cells. *Nat. Genet.* **49**, 1779–1784 (2017).
66. J. M. Dempster *et al.*, Extracting biological insights from the project Achilles genome-scale CRISPR screens in cancer cell lines. bioRxiv:10.1101, 720243 (31 July 2019).
67. Broad DepMap, DepMap 20Q4 Public. Figshare. https://doi.org/10.6084/m9.figshare.13237076.v2. Deposited 13 November 2020.
68. J. Cai *et al.*, Two distinct molecular mechanisms underlying cytarabine resistance in human leukemic cells. *Cancer Res.* **68**, 2349–2357 (2008).
69. Y. Liu, T. Zuo, X. Zhu, N. Ahuja, T. Fu, Differential expression of hENT1 and hENT2 in colon cancer cell lines. *Genet. Mol. Res.* **16**, gmr16019549 (2017).
70. X. N. Pan *et al.*, Inhibition of c-Myc overcomes cytotoxic drug resistance in acute myeloid leukemia cells by promoting differentiation. *PloS One* **9**, e105381 (2014).
71. A. Porro *et al.*, C-MYC oncoprotein dictates transcriptional profiles of ATP-binding cassette transporter genes in chronic myelogenous leukemia CD34+ hematopoietic progenitor cells. *Mol. Canc. Res.* **9**, 1054–1066 (2011).
72. C. D. Drenberg *et al.*, ABCC4 is a determinant of cytarabine-induced cytotoxicity and myelosuppression. *Clin. Transl. Sci.* **9**, 51–59 (2016).
73. J. Furukawa *et al.*, Functional identification of SLC43A3 as an equilibrative nucleobase transporter involved in purine salvage in mammals. *Sci. Rep.* **5**, 15057 (2015).
74. Y. D. Bhutia, E. Babu, S. Ramachandran, V. Ganapathy, Amino acid transporters in cancer and their relevance to "glutamine addiction": Novel targets for the design of a new class of anticancer drugs. *Cancer Res.* **75**, 1782–1788 (2015).
75. Y. D. Bhutia, V. Ganapathy, Glutamine transporters in mammalian cells and their functions in physiology and cancer. *Biochim. Biophys. Acta* **1863**, 2531–2539 (2016).
76. M. Hassanein *et al.*, SLC1A5 mediates glutamine transport required for lung cancer cell growth and survival. *Clin. Canc. Res.* **19**, 560–570 (2013).
77. M. Van Geldermalsen *et al.*, ASCT2/SLC1A5 controls glutamine uptake and tumour growth in triple-negative basal-like breast cancer. *Oncogene* **35**, 3201–3208 (2016).

78. F. D. de Carvalho, M. Quick, Surprising substrate versatility in SLC5A6: Na+-coupled I- transport by the human Na+/multivitamin transporter (hSMVT). *J. Biol. Chem.* **286**, 131–137 (2011).
79. C. Huang, X. Cui, X. Sun, J. Yang, M. Li, Zinc transporters are differentially expressed in human non-small cell lung cancer. *Oncotarget* **7**, 66935–66943 (2016).
80. M. Yue, J. Jiang, P. Gao, H. Liu, G. Qing, Oncogenic MYC activates a feedforward regulatory loop promoting essential amino acid metabolism and tumorigenesis. *Cell Rep.* **21**, 3819–3832 (2017).
81. M. R. Wu *et al.*, B7H6-specific bispecific T cell engagers lead to tumor elimination and host antitumor immunity. *J. Immunol.* **194**, 5305–5311 (2015).
82. D. S. Askew, R. A. Ashmun, B. C. Simmons, J. L. Cleveland, Constitutive c-myc expression in an IL-3-dependent myeloid cell line suppresses cell cycle arrest and accelerates apoptosis. *Oncogene* **6**, 1915–1922 (1991).
83. A. Amanullah, D. A. Liebermann, B. Hoffman, Deregulated c-Myc prematurely recruits both type I and II CD95/Fas apoptotic pathways associated with terminal myeloid differentiation. *Oncogene* **21**, 1600–1610 (2002).
84. Z. Cheng *et al.*, Inhibition of BET bromodomain targets genetically diverse glioblastoma. *Clin. Canc. Res.* **19**, 1748–1759 (2013).
85. H. Zhang, X. J. Li, D. B. Martin, R. Aebersold, Identification and quantification of N-linked glycoproteins using hydrazide chemistry, stable isotope labeling and mass spectrometry. *Nat. Biotechnol.* **21**, 660–666 (2003).
86. J. Wei *et al.*, Profiling the surfaceome identifies therapeutic targets for cells with hyperactive mTORC1 signaling. *Mol. Cell. Proteomics* **19**, 294–307 (2020).
87. B. MacLean *et al.*, Skyline: An open source document editor for creating and analyzing targeted proteomics experiments. *Bioinformatics* **26**, 966–968 (2010).
88. H. Persson *et al.*, CDR-H3 diversity is not required for antigen recognition by synthetic antibodies. *J. Mol. Biol.* **425**, 803–811 (2013).